ALKBH5 Regulates Corneal Neovascularization by Mediating FOXM1 M6A Demethylation

Wei Wang,[1] Hua Li,[1] Yiyong Qian,[1] Min Li,[1] Manli Deng,[1] Dexi Bi,[2] and Jun Zou[1]

[1]Department of Ophthalmology, Shanghai Tenth People's Hospital, School of Medicine, Tongji University, Shanghai, China
[2]Department of Pathology, Shanghai Tenth People's Hospital, School of Medicine, Tongji University, Shanghai, China

Correspondence: Dexi Bi, Department of Pathology, Shanghai Tenth People's Hospital, School of Medicine, Tongji University, Shanghai 200072, China; bidexi@tongji.edu.cn.
Jun Zou, Department of Ophthalmology, Shanghai Tenth People's Hospital, School of Medicine, Tongji University, Shanghai 200072, China; zoujun70@126.com.

WW and HL are joint first authors.

Received: August 14, 2024
Accepted: September 30, 2024
Published: October 23, 2024

Citation: Wang W, Li H, Qian Y, et al. ALKBH5 regulates corneal neovascularization by mediating FOXM1 M6A demethylation. *Invest Ophthalmol Vis Sci.* 2024;65(12):34. https://doi.org/10.1167/iovs.65.12.34

Purpose. This study aims to explore the regulatory role and potential mechanisms of ALKBH5-mediated N6-methyladenosine (m6A) demethylation modification in corneal neovascularization (CNV).

Methods. A mouse CNV model was established through corneal alkali burns. Total m6A levels were measured using an m6A RNA methylation quantification kit. The mRNA expression of candidate m6A-related enzymes was quantified by quantitative RT–PCR. Small interfering RNA targeting ALKBH5 was injected subconjunctivally into alkali-burned mice. The CNV area, corneal epithelial thickness, and pathological changes were evaluated. Protein expression was detected by western blot and immunofluorescence. Human umbilical vein endothelial cells (HUVECs) were treated with IL-6. Plasmid transfection knocked down ALKBH5 or overexpressed FOXM1 in IL-6–induced HUVECs. The assays of CCK8, wound healing, and tube formation evaluated the cell proliferation, migration, and tube formation abilities, respectively. The dual-luciferase assay examined the binding between ALKBH5 and FOXM1. Methylated RNA immunoprecipitation–qPCR detected the m6A levels of FOXM1.

Results. Significant CNV was observed on the seventh day. Total m6A levels were reduced, and ALKBH5 expression was increased in CNV corneas and IL-6–induced HUVECs. ALKBH5 knockdown alleviated corneal neovascularization and inflammation and countered IL-6–induced promotion of cell proliferation, migration, and tube formation in HUVECs. ALKBH5 depletion increased m6A levels and decreased VEGFA and CD31 expression both in vivo and in vitro. This knockdown in HUVECs elevated m6A levels on FOXM1 mRNA while reducing its mRNA and protein expression. Notably, FOXM1 overexpression can reverse ALKBH5 depletion effects.

Conclusions. ALKBH5 modulates FOXM1 m6A demethylation, influencing CNV progression and highlighting its potential as a therapeutic target.

Keywords: ALKBH5, FOXM1, m6A, demethylation, corneal neovascularization

The cornea is typically avascular and maintained by a delicate balance between pro-angiogenic and anti-angiogenic factors. The balance, however, can be disrupted by various hazardous factors, such as trauma, inflammation, infection, chemical burns, hypoxia, and allergy.[1] Under such circumstances, new capillaries from the limbus invade the cornea and result in corneal neovascularization (CNV), which is a pathological condition that affects corneal transparency and impairs vision in severe cases.[2] Current treatment strategies for CNV focus on anti-inflammatory and anti-angiogenic approaches.[3] However, long-term use of steroids may lead to side effects such as glaucoma, cataracts, and secondary infections. Additionally, the effectiveness of anti-vascular endothelial growth factor (VEGF) drugs is limited in chronic CNV cases.[4,5] Therefore, exploring the pathogenesis of CNV is crucial for guiding clinical treatment and effectively preventing corneal blindness.

N6-methyladenosine (m6A), a methylation modification that occurs on the sixth nitrogen atom of adenine in RNA, is the most abundant internal RNA modification in eukaryotes and an important focus in epigenetic research. This process is dynamic and reversible, regulated by m6A methyltransferases (METTL3, METTL14, and WTAP), demethylases (FTO, ALKBH5), and binding proteins (YTHDFs, YTHDCs, IGF2BPs, and HNRNPC/G/A2B1).[6,7] Evidence indicates that m6A modifications govern various aspects of RNA processing, including splicing, nuclear exports, stability, translation, localization, and decay.[8] According to previous studies, aberrant m6A modification and dysregulated m6A-related enzymes are associated with CNV.[9–12] In suture-induced mouse CNV, m6A levels decrease. Silencing FTO can inhibit CNV progression and regulate the function of human umbilical vein endothelial cells (HUVECs) in an m6A-YTHDF2-dependent manner.[10] However, the specific contribution of

m6A modification to the development of CNV has just now begun to surface.

ALKBH5, the second discovered m6A demethylase to date, directly reverses m6A to adenosine and regulates a wide range of biological processes such as proliferation, migration, invasion, and metastasis.[13] In recent years, extensive research has provided compelling evidence for the association between ALKBH5 and pathological angiogenesis. For example, in human myeloma cell lines, ALKBH5 promotes angiogenesis by modulating SAV1, which is a core member of the Hippo pathway.[14] In the context of acute ischemic stress, inhibiting ALKBH5 substantially elevates the m6A levels of SPHK1 mRNA and modulates the downstream eNOS-AKT signaling pathway, thereby impairing endothelial cell angiogenesis.[15] Furthermore, ALKBH5 modulates the stability of PIK3C2B mRNA through its demethylation activity, which activates the AKT/mTOR signaling pathway in retinal pigment epithelial cells, thus fostering choroidal neovascularization.[16] These findings collectively show that targeting ALKBH5 as a therapeutic approach holds potential for neovascularization, yet currently, there have been no reports on the involvement of the m6A demethylase ALKBH5 in CNV.

FOXM1 (forkhead box M1) is a transcription factor intricately linked to cell proliferation and angiogenesis, displaying widespread spatiotemporal expression throughout the cell cycle.[17] It is frequently overexpressed in various human cancers and plays a pivotal role in regulating VEGF-A expression, promoting tumorigenic angiogenesis by binding to the VEGF-A promoter and activating its transcription.[18,19] Recent studies have reported that an inhibitor targeting the forkhead domain can effectively suppress alkali burn–induced CNV.[20] Interestingly, the stability and expression activity of FOXM1 are regulated by m6A modification. In glioblastoma stem-like cells, FOXM1 occupies a central position in the downstream signaling pathway of ALKBH5.[21] Using the SRAMP database, we predicted multiple m6A modification sites on FOXM1 mRNA. Therefore we are interested in investigating whether ALKBH5 regulates CNV process by modulating m6A demethylation modification of FOXM1 mRNA. This study investigates the regulatory role and mechanisms of the m6A demethylase ALKBH5 in CNV and IL-6-induced HUVECs, proposing a possible anti-angiogenic treatment target for CNV patients from the perspective of epigenetic regulation.

Material and Methods

Mice

A total of 96 eight-week-old female BALB/c mice were used in this study. They were kept in the laboratory animal center of Tongji University and housed in separate cages with six mice per cage on a 12-hour light/dark cycle. The environmental conditions were maintained at 25°C and 60% air humidity. Before the experiment began, all mice underwent one week of adaptive feeding and underwent regular slit-lamp examinations to rule out any current ocular diseases. This research adhered to the Association for Research in Vision and Ophthalmology (ARVO) Statements for the Use of Animals in Ophthalmology and Vision Research. All animal experiments were approved by the Animal Ethics Committee of Shanghai Tenth People's Hospital (ID Number: SHDSYY-2024-3503). In compliance with ethical guidelines, mice were euthanized by an overdose injection of pentobarbital solution.

Alkali Burn-Induced Corneal Neovascularization

General anesthesia in mice was induced by intraperitoneal injection of a 0.3% pentobarbital sodium solution at 40 mg/kg. Excessive whiskers were trimmed, and topical anesthesia was performed using 0.5% proparacaine hydrochloride (Alcon, Geneva, Switzerland). A circular filter paper (2.0 mm × 2.0 mm) soaked with NaOH (1 mol/L) was attached to the central cornea of the right eye for 40 seconds to induce an alkali injury. Afterward, the paper was quickly removed, and the conjunctival sac was washed entirely with 0.9% sterile saline solution for one minute. Mice were then treated with ofloxacin eye drops twice daily for three days to prevent infection. Mice were randomly selected for three, seven, and 14 days or seven days after modeling, and their right corneas were harvested for subsequent experiments.

In Vivo Slit-Lamp Evaluation of Mice Corneas

On days 3, 7, and 14, or on day 7 after alkali burn, corneal images were observed and captured using a slit-lamp microscope equipped with a digital camera in a darkroom. These images included frontal views for measuring CNV area and lateral views for analyzing CNV length (distance from the limbus to vessel tips) using a free-hand tool in ImageJ software.

Subconjunctival Injection of SiRNA

The subconjunctival injection technique facilitates controlled dispersion of the administered substance into the cornea while mitigating systemic side effects. The small interfering RNA (siRNA) targeting ALKBH5 in vivo (siALKBH5; AM16831) was procured from Ambion (ThermoFisher, St. Louis, MO, USA) and prepared in solution according to the supplier's instructions before use. One hour and three days after corneal alkali burns, a 33-gauge Hamilton syringe needle was carefully inserted to administer the siRNA solution (10 µmol/L, 5 µL per eye) subconjunctivally into the right eye of the anesthetized animal under ophthalmic microscope guidance. Then, a drop of siRNA was instilled into the right eye twice daily for seven days to augment knockdown efficiency. To serve as a negative control, equivalent volumes of physiological saline were subconjunctivally injected using the same method.

Hematoxylin-Eosin Staining

After corneal alkali burns, the right eyeballs of mice were extracted for hematoxylin-eosin (H&E) staining at the indicated time points. They were fixed in 4% paraformaldehyde for 48 hours and then subjected to routine paraffin embedding. The cornea was sagittally sectioned parallel to the optic nerve head, and consecutive slices were taken from the corneal edge toward the center, with each slice approximately 5 µm thick. Hematoxylin and eosin were used to stain three randomly selected paraffin sections from each group before being observed and captured under a microscope (Nikon Inc., Melville, NY, USA). The images will be used for analyzing corneal epithelial thickness using ImageJ.

Investigative Ophthalmology & Visual Science

Immunohistofluorescence Staining

When conducting immunohistofluorescence (IHF) staining, tissues were first fixed in 4% paraformaldehyde for 1 hour, followed by incubation at 37°C in a solution containing 0.1% Triton X-100 (ThermoFisher) and 5% BSA (Sigma-Aldrich Corp., St. Louis, MO, USA) for 30 minutes. Primary antibodies, including anti-ALKBH5 (ab195377, 1:200; Abcam, Cambridge, MA, USA), anti-VEGF-A (ab52917, 1:200; Abcam), anti-CD31 (ab281583, 1:50; Abcam), anti-K14 (ab181595, 1:200; Abcam), anti-MPO (ab208670, 1:100; Abcam), and anti-F4/80 (ab300421, 1:100; Abcam) were applied overnight at 4°C, followed by three washes with PBS. Subsequently, Alexa Fluor 488 or Alexa Fluor 594 secondary antibodies (1:200; ThermoFisher) were applied for one hour at room temperature. DAPI was used for nuclear staining. Finally, an anti-fluorescence quench agent was used to seal the slides. Images were captured using a fluorescence microscope (Nikon) controlled by TissueFAXS software. The average fluorescence intensity of the images was automatically calculated by ImageJ, with DAPI's average fluorescence intensity serving as reference. Only minor adjustments to brightness and contrast were applied to the images. For co-localization studies, the Coloc 2 plugin in ImageJ was used to assess the Pearson's coefficient,[22] which ranges from 1 (perfect correlation) to −1 (perfect negative correlation), with 0 indicating no association.[23]

Cell Culture and Treatment

HUVECs, a well-established model cell for investigating vascular endothelial properties and angiogenesis in vitro, were obtained from the American Type Culture Collection. The cells were cultured in DEME medium (Gibco, Thermo Fisher Scientific, Waltham, MA, USA), supplemented with 10% FBS (Gibco, Thermo Fisher Scientific) and 1% penicillin-streptomycin (Gibco, Thermo Fisher Scientific), and maintained in a 5% CO_2 incubator at 37°C. For the experiments, cells within the three to eight passages were used. To establish the high-IL-6 group, the cells were starved in FBS-free DEME for 24 hours before adding IL-6 (Peprotech, Cranbury, NJ, USA).

Cell Transfection

For gene silencing, ALKBH5 siRNA (siALKBH5) and negative control siRNA (siNC) plasmids were purchased from GeneChem (Shanghai, China). Following the manufacturer's established protocols, HUVECs were transfected with the plasmids using Lipofectamine 2000 (ThermoFisher). After a 48-hour incubation period, cells were harvested for subsequent experimental procedures. The designed sequences were as follows:

siALKBH5: 5′-GGGAGAAGCTCAAGTCCATGA-3′
Flag-FOXM1: 5′-ATGAAAACTAGCCCCCGTCGGCC-3′

CCK8 Assay

The viability of HUVECs was assessed by CCK8 (Beyotime Institute of Biotechnology, Jiangsu, China). A total of 3000 cells in 100 µL of culture medium were seeded into each well of a 96-well plate and incubated for 24 hours. After the designated treatment, 10 µL of CCK8 solution was added to each well at 37°C for a one-hour reaction under light-protected conditions. The optical density (OD) at 450 nm was measured using a microtiter plate reader (ThermoFisher).

Wound Healing Assay (Scratch Assay)

HUVECs were seeded in six-well plates and cultured until reaching 80% confluence. To create wounds, a precise incision was made at the center of the confluent cell monolayer using a 200 µL sterile pipette tip, followed by gentle washing with PBS to remove detached cells. The closure dynamics of the wounds were monitored at both 0 and 24 hours, and images were captured using an inverted microscope equipped with a digital camera (Nikon). The remaining wound area was quantified using Image J software. The wound healing rate was calculated as follows: (Wound area at 0 hours − Wound area at 24 hours)/Wound area at 0 hours × 100%, as previously mentioned.[24]

Tube Formation Assay

After transfection with siALKBH5, cells were seeded onto 96-well plates pre-coated with 50 µL of Matrigel (Corning Inc., Corning, NY, USA), ensuring no bubble formation. Matrigel was diluted with DMEM in a 1:1 ratio and solidified after a 30-minute incubation at 37°C. After four hours, the formation of capillary-like structures was examined and photographed under an optical microscope. Capillary lengths (i.e., Tot. branching length) and branch points (i.e., Nb branches) were quantified automatically using ImageJ with the angiogenesis analyzer plugin.

Dual-Luciferase Reporter Assay

HUVECs treated with IL-6 underwent co-transfection procedures, where either wild-type (WT) or mutant (MUT) FOXM1-mouse 3′UTR was transfected along with siALKBH5 or siNC using Lipofectamine 2000. Customized FOXM1-WT and FOXM1-MUT constructs were purchased from GeneChem (Shanghai, China). Subsequently, the cells were incubated for 48 hours after transfection. Luciferase activity was then assayed using the Dual Luciferase Reporter Gene Assay Kit (Beyotime Institute of Biotechnology). Luminescence signals were then captured using the SpectraMax iD5 Multi-Mode Microplate Reader (Molecular Devices, San Jose, CA, USA). For each sample, the luminescence ratio of Firefly Luciferase to Renilla Luciferase was calculated. The designed sequences were as follows:

FOXM1-WT: 5′-AGCATCAGGGACTGAGGAGCC-3′
FOXM1-MUT: 5′-AGCATCAGGGTCTGAGGAGCC-3′

M6A RNA Methylation Quantification

The total m6A levels of extracted RNA were measured using an EpiQuik m6A RNA Methylation Quantification Kit (Colorimetric; EpiGentek, Farmingdale, NY, USA). For each sample, 200 ng of RNA was added to the assay wells. The detection antibody solution, appropriately diluted as per the manufacturer's instructions, was then added to the test wells. The m6A levels were quantified by measuring the absorbance at a wavelength of 450 nm in each well, and the m6A level was calculated based on the standard curve.

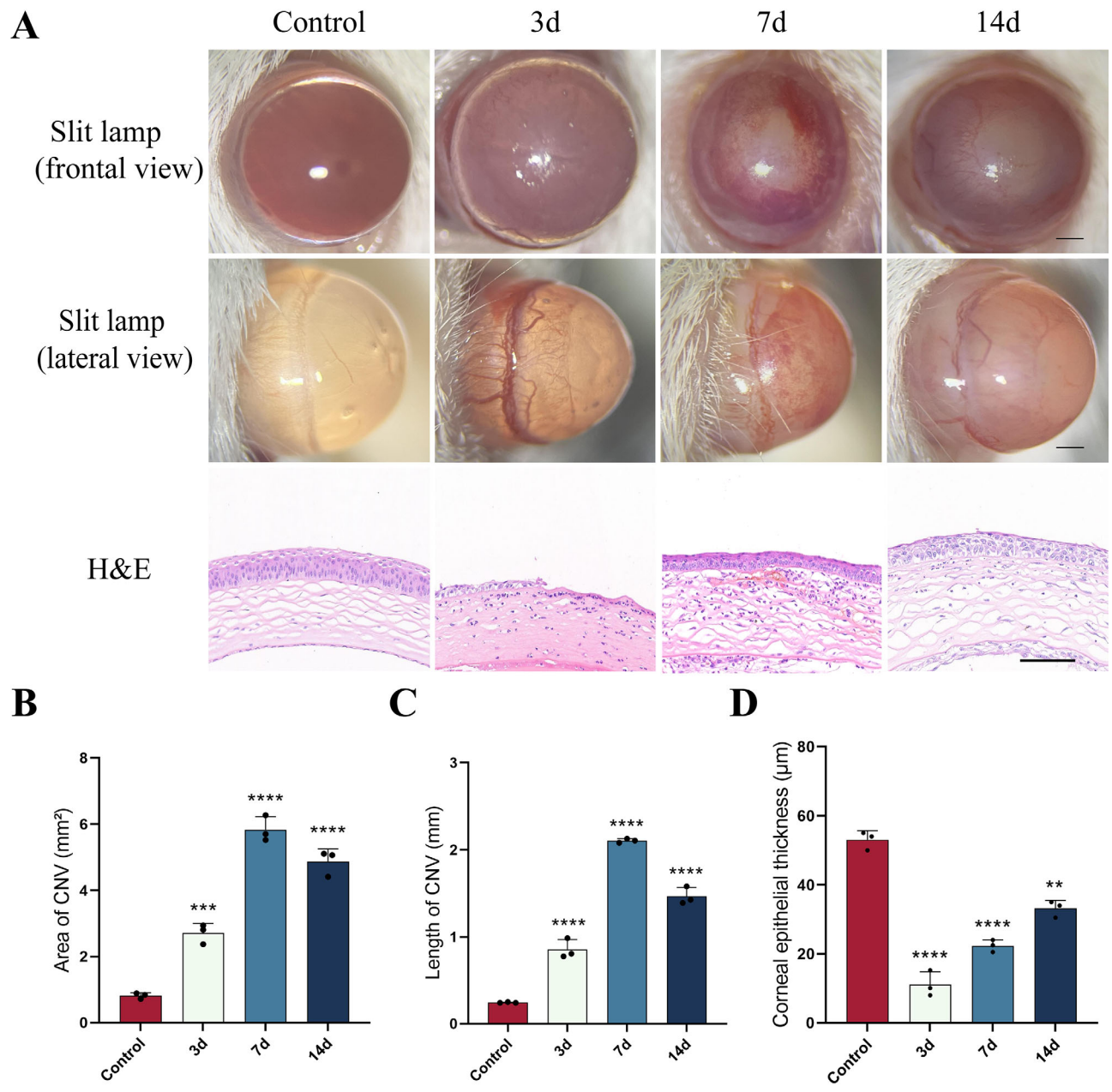

Figure 1. The 14-day monitoring of the mouse corneal alkali burns model. (**A**) Representative images of the cornea obtained through slit-lamp examination (*top two rows*, *scale bar:* 0.5 mm) and HE staining (*bottom row*, *scale bar:* 100 μm), $n = 12$. (**B–D**) Quantification results of CNV area, length, and corneal epithelial thickness. n is the total number of test animals used. $^{**}P < 0.01$, $^{***}P < 0.001$, $^{****}P < 0.0001$, compared with the control group.

Immunocytofluorescence Staining

HUVECs were cultured in a 24-well plate, and cell slides were prepared for immunocytofluorescence (ICF) staining. These slides were fixed with 4% paraformaldehyde at room temperature for 20 minutes, permeabilized with 0.1% Triton X-100 (ThermoFisher) for five minutes, and then blocked with 5% BSA (Sigma-Aldrich) for 30 minutes. Primary antibodies, including anti-VEGF-A (ab52917, 1:250; Abcam) and anti-CD31 (ab9498, 1 μg/mL; Abcam), were subsequently added to the slides, followed by overnight incubation at 4°C in a humid chamber. Following this step, the slides underwent incubation with Alexa Fluor 594 secondary antibodies (1:200; ThermoFisher) at room temperature in the dark for one hour. Finally, the nucleus was stained with DAPI for 10 minutes. Slides were observed, and images were captured under a fluorescence microscope (Nikon) using CaseViewer software. The average fluorescence intensity of the images was automatically calculated by ImageJ, with DAPI's average fluorescence intensity serving as reference.

Western Blot Analysis

Tissue and cell proteins were lysed using a cold radioimmunoprecipitation assay (RIPA) buffer (Beyotime Institute of Biotechnology) and supplemented with phenylmethane

Investigative Ophthalmology & Visual Science

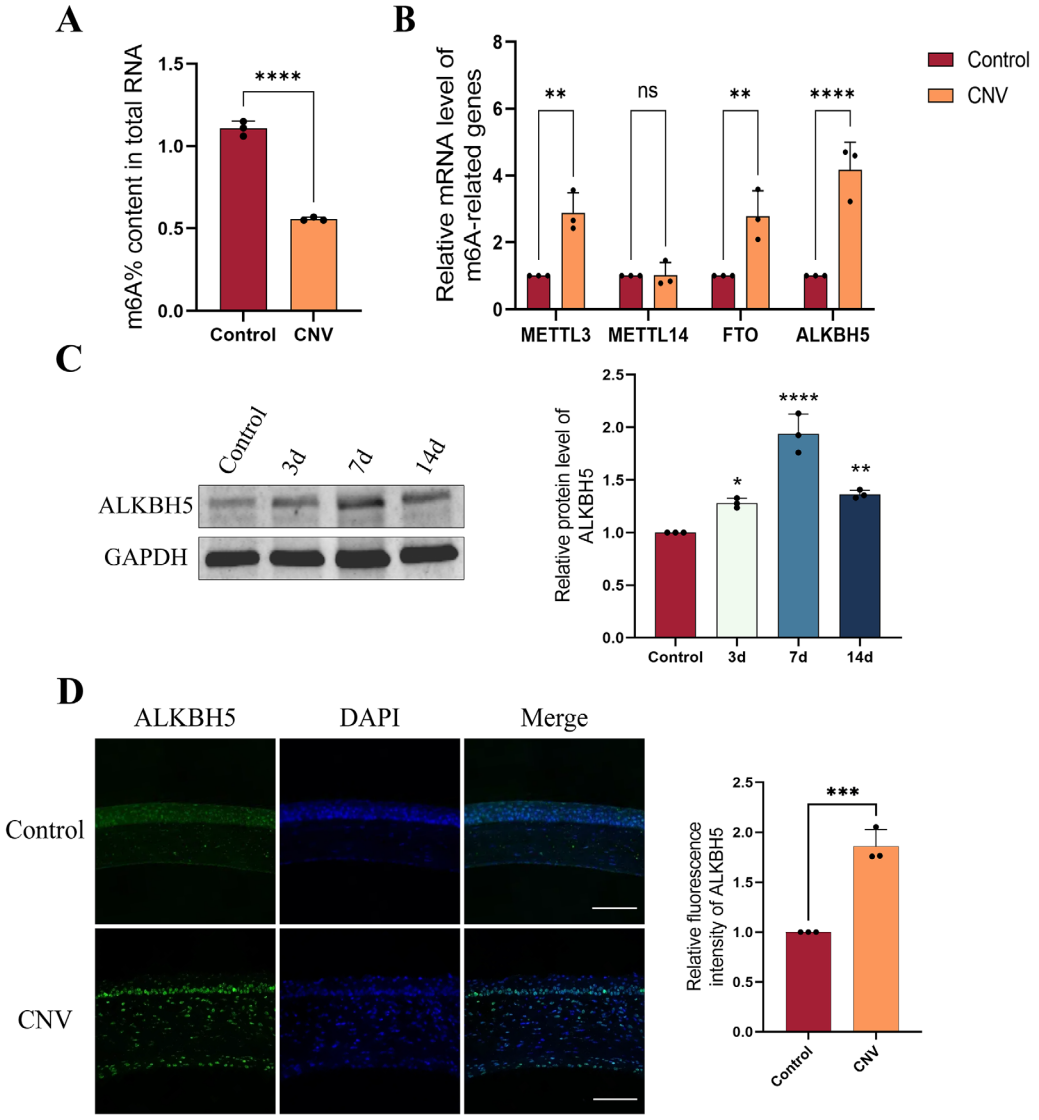

Figure 2. Downregulated m6A levels and upregulated ALKBH5 expression in CNV corneas. (**A**) Quantitative analysis of total m6A levels in normal and CNV corneas ($n = 6$). (**B**) The qRT–PCR analysis of candidate m6A-related enzymes in normal and CNV corneas, with the fold ratio of the control group normalized to 1 ($n = 6$). (**C**) Western blot analysis (*left graph*) and quantitative analysis (*right graph*) of ALKBH5 protein levels in corneas on days 3, 7, and 14 after alkali burns, with the fold ratio of the control group normalized to 1 ($n = 12$). (**D**) IHF analysis (*left graph*) and quantitative analysis (*right graph*) of ALKBH5 in normal and CNV corneas ($n = 6$). ALKBH5, *green*; nucleus, *blue*. *Scale bar:* 100 µm. *n* is the total number of test animals used. $^{*}P < 0.05$, $^{**}P < 0.01$, $^{***}P < 0.001$, $^{****}P < 0.0001$; ns, no significant difference, compared with the control group.

sulfonyl fluoride (Beyotime Institute of Biotechnology), a commonly employed serine protease inhibitor, on ice for 15 minutes. Then the lysis mixtures underwent centrifugation at 14,000*g* for 10 minutes at 4°C, and the resultant supernatants were collected for protein concentration determination using the BCA protein assay kit (Beyotime Institute of Biotechnology). After performing 8%, 10%, or 12% SDS-PAGE electrophoresis, the proteins were transferred onto a PVDF membrane, which was then blocked by a 5% BSA solution for one hour. Subsequently, the membranes were incubated overnight at 4°C with primary antibodies, including anti-ALKBH5 (ab195377, 1:1000; Abcam), anti-FOXM1 (no. 3948, 1:1000; Cell Signaling Technology, Danvers, MA, USA), anti-IL-6 (ab290735, 1:1000; Abcam), anti-IL-1β (ab315084, 1:1000; Abcam), anti-VEGFA (ab214424, 1:1000; Abcam), and anti-CD31 (ab281583, 1:1000; Abcam). Anti-β-actin (ab179467, 1:5000; Abcam) and anti-GAPDH (ab181603, 1:10000; Abcam) were used as protein loading controls. Afterward, the membranes were incubated with fluorescent secondary antibodies at room temperature in the dark for one hour. The specific bands were detected using the LI-COR Odyssey CLx scanner (LI-COR Biosciences, Lincoln, NE, USA), and quantification was analyzed with ImageJ.

Quantitative Real-Time PCR (qRT–PCR) Analysis

Total RNA was extracted from selected cells or tissues using TRIzol reagent (Beyotime Institute of Biotechnology). The cDNA templates were synthesized using HiScript II reverse transcriptase (Vazyme Biotech Co., Ltd, Nanjing, China). Subsequently, qRT–PCR was performed using 2 × AceQ

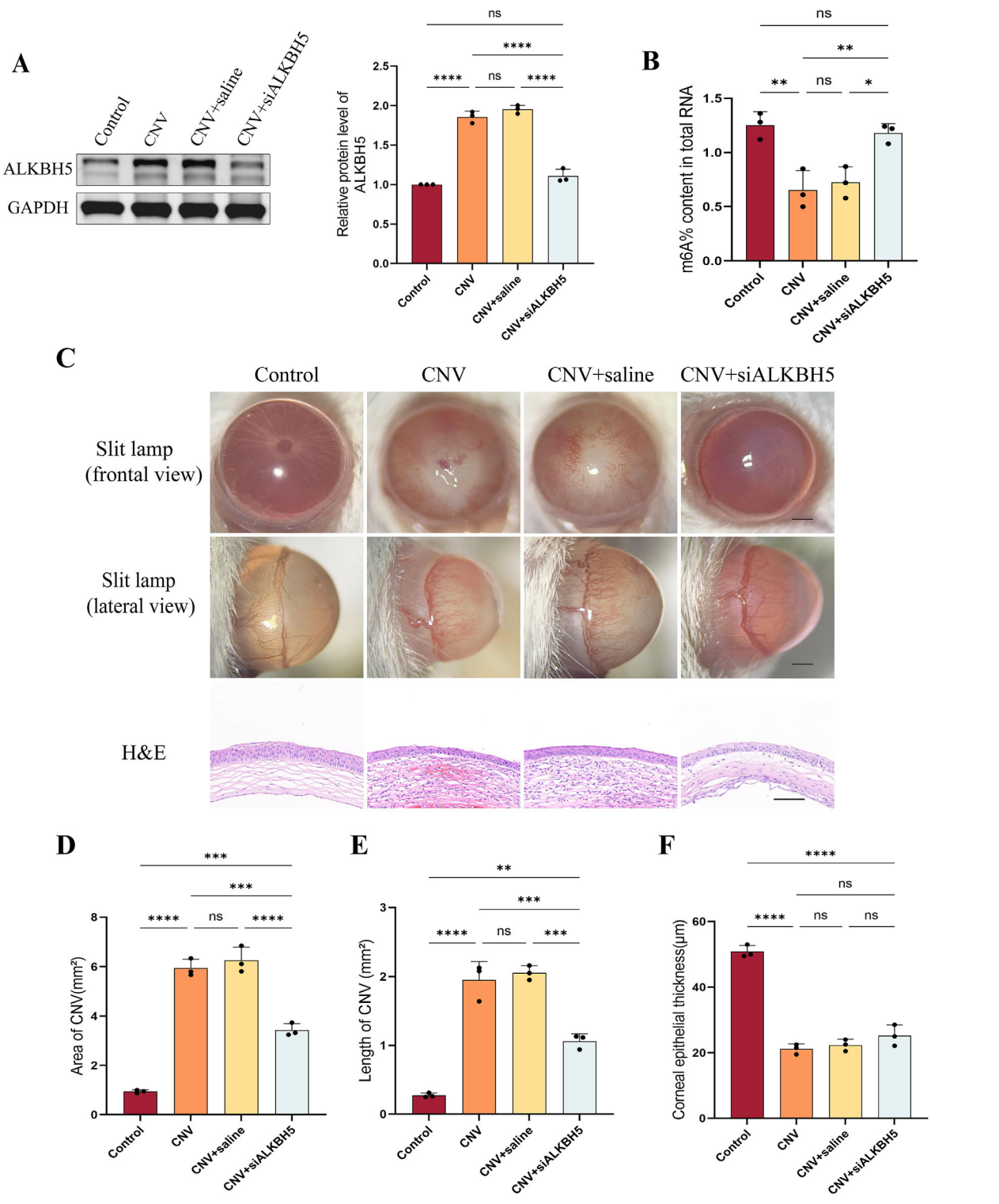

Figure 3. Subconjunctival injection of siALKBH5 alleviates CNV in vivo. (**A**) Western blot analysis (*left graph*) and quantitative analysis (*right graph*) of ALKBH5 protein levels in the control group, CNV group, CNV + saline group, and CNV + siALKBH5 group, with the fold ratio of the control group normalized to 1 ($n = 12$). (**B**) Quantitative analysis of total m6A levels in four groups ($n = 12$). (**C**) Representative images of the cornea obtained through slit-lamp examination (*top two rows, scale bar:* 0.5 mm) and HE staining (*bottom row, scale bar:* 100 μm) in four groups, $n = 12$. (**D–F**) Quantitative analysis of CNV area, length, and corneal epithelial thickness in four groups, with the fold ratio of the control group set to 1. (**G**) Western blot analysis (*leftmost image*) and quantitative analysis (*right two images*) of VEGF-A and CD31 protein levels in four groups, with the fold ratio of the control group normalized to 1. (**H, I**) IHF analysis (*left graph*) and quantitative analysis (*right graph*) of VEGF-A and CD31 in four groups. The relative fluorescence intensity was determined by comparing the average fluorescence intensity values of the samples, expressed as folds relative to the control ($n = 12$). VEGF-A and CD31, *green*; nucleus, *blue*. *Scale bar:* 20 μm. n is the total number of test animals used. $^{*}P < 0.05$, $^{**}P < 0.01$, $^{***}P < 0.001$, $^{****}P < 0.0001$; ns, no significant difference.

Investigative Ophthalmology & Visual Science

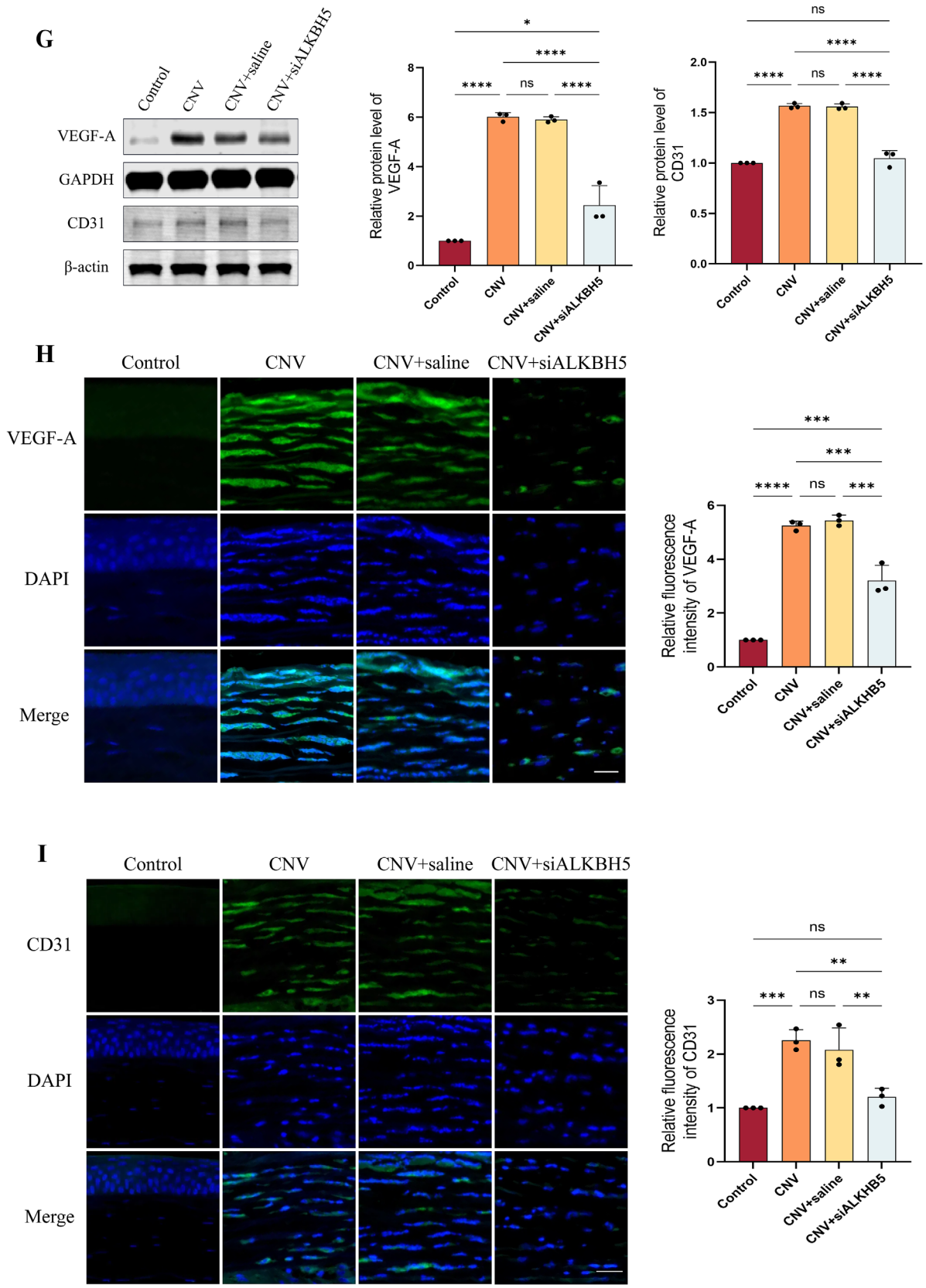

Figure 3. Continued.

Investigative Ophthalmology & Visual Science

qPCR SYBR Green Master Mix (Vazyme Biotech Co.) on ABI QuantStudio Dx Real-Time PCR instruments (Thermo Fisher, St. Louis, MO, USA) in accordance with established protocols. The relative expression levels of target genes were calculated based on the $2^{-\Delta\Delta Ct}$ method, with GAPDH serving as an internal reference gene. The primer sequences used in this study are listed in Supplementary Table S1.

Sequence-Based RNA Adenosine Methylation Site Predictor Analysis

The sequence-based RNA adenosine methylation site predictor (SRAMP, http://www.cuilab.cn/sramp/) was used to predict m6A modification sites.[25] The FOXM1 mRNA sequence was received from the National Center for Biotechnology Information and examined in mature mRNA mode. After inputting the query sequence, SRAMP provides a prediction score for the predicted m6A modification sites. The thresholds for very high-, high-, moderate-, and low-confidence m6A sites correspond to the 99%, 95%, 90%, and 85% specificities in the cross-validation tests, respectively. The most likely m6A binding site was predicted based on the highest combined prediction score by three random forest classifiers.

Methylated RNA Immunoprecipitation (MeRIP)–qPCR

The MeRIP assay was conducted using the Magna MeRIP m6A Kit (Millipore, Burlington, MA, USA) following the manufacturer's protocol. In brief, 200 µg of total RNA was extracted from HUVECs and mouse corneal samples of each group. The chemically fragmented RNA (about 200 nucleotides) was then incubated with anti-m6A antibody (ab151230, 1:500; Abcam) or anti-IgG antibody (ab133470, 1:100; Abcam)-conjugated beads in 500 µL of 1 × IP buffer containing RNase inhibitors at 4°Covernight. Methylated RNA was immunoprecipitated with the beads, eluted through competition with free m6A, and purified using the RNeasy Mini Kit (Qiagen, Hilden, Germany). The m6A enrichment was assessed in each sample by qRT–PCR and normalized to input.

Statistical Analysis

Statistical analyses were conducted using GraphPad Prism software (version 9.5.1; GraphPad, San Diego, CA, USA). Data were derived from at least three independent experiments and were expressed as mean ± standard deviation (SD). For normally distributed data, comparisons between two groups were assessed using a two-tailed unpaired *t*-test, and multiple group comparisons were performed using a one-way analysis of variance. A significance threshold of $P < 0.05$ was applied to determine statistical significance.

Results

Dynamic Corneal Changes in the Mouse Model of Alkali Burns Reveal Peak Neovascularization on Day 7

To assess corneal changes induced by alkali burns in mice, we monitored the CNV progression on days 3, 7, and 14. The results showed that neovascularization progressively encroached toward the central cornea, reaching its maximum area and length on day 7 and showing moderate alleviation on day 14 (Figs. 1A–C). HE staining showed that on day 3, the epithelium was severely damaged; however, by day 7, corneal re-epithelialization occurred (Figs. 1A, 1D). Moreover, the most pronounced histological changes were evident on day 7 after alkali burns, characterized by prominent infiltration of inflammatory cells, stromal edema and thickening, and extensive neovascularization (Fig. 1A). Considering the peak CNV observed on day 7, the corneal tissues from this time point were chosen for further study.

Downregulated M6A Levels and Upregulated ALKBH5 Expression in CNV Corneas

The overall m6A levels were assessed to uncover the m6A modification patterns in normal and CNV corneas. Quantitative analysis revealed a reduction in m6A abundance in CNV corneas compared to normal ones (Fig. 2A). After this, we used qRT–PCR to investigate the expression profiles of various known methyltransferases, METTL3 and METTL14, as well as demethylases, FTO and ALKBH5. Notably, the expression of METTL3, FTO, and ALKBH5 was significantly elevated in CNV corneas, with ALKBH5 showing the most pronounced increase, whereas METTL14 expression remained unaltered (Fig. 2B). Given that limited information is available regarding the mechanism of action of ALKBH5 in CNV, it became the primary focus of our study. We then verified the trend of ALKBH5 expression on different monitoring days in this model. Interestingly, ALKBH5 expression showed a pattern that coincided with the severity of CNV: peaking on day 7 and slightly decreasing on day 14 (Fig. 2C). IHF analysis further demonstrated that ALKBH5 expression was more widely distributed in CNV corneas on day 7, spanning all layers of the cornea, than in control mice (Fig. 2D).

Next, immunofluorescent co-localization was performed to determine the major cellular source of ALKBH5 and m6A. Four protein markers, namely CD31, K14, MPO, and F4/80, were used for this purpose (Supplementary Fig. S1A). The degree of co-localization between ALKBH5 and these markers was quantified using Pearson's coefficient (Supplementary Fig. S1B). The results indicate that ALKBH5 exhibits the most significant co-localization with CD31, suggesting its primary expression in corneal vascular endothelial cells. Overall, our data strongly support the role of ALKBH5 as a crucial regulatory factor influencing aberrant m6A modification levels in CNV.

Subconjunctival Injection of siALKBH5 Alleviates CNV In Vivo

To investigate the regulatory role of ALKBH5 in vivo, siALKBH5 was injected into the subconjunctiva of alkali-burned mice. Western blot results confirmed a decrease in ALKBH5 protein levels, contributing to elevated m6A levels post-siRNA injection (Figs. 3A, 3B). Additionally, ALKBH5 inhibition resulted in a significant reduction in neovascularization area and length, alleviating inflammation cell infiltration, with no significant difference detected between the CNV group and the CNV + saline group (Figs. 3C–E).

Investigative Ophthalmology & Visual Science

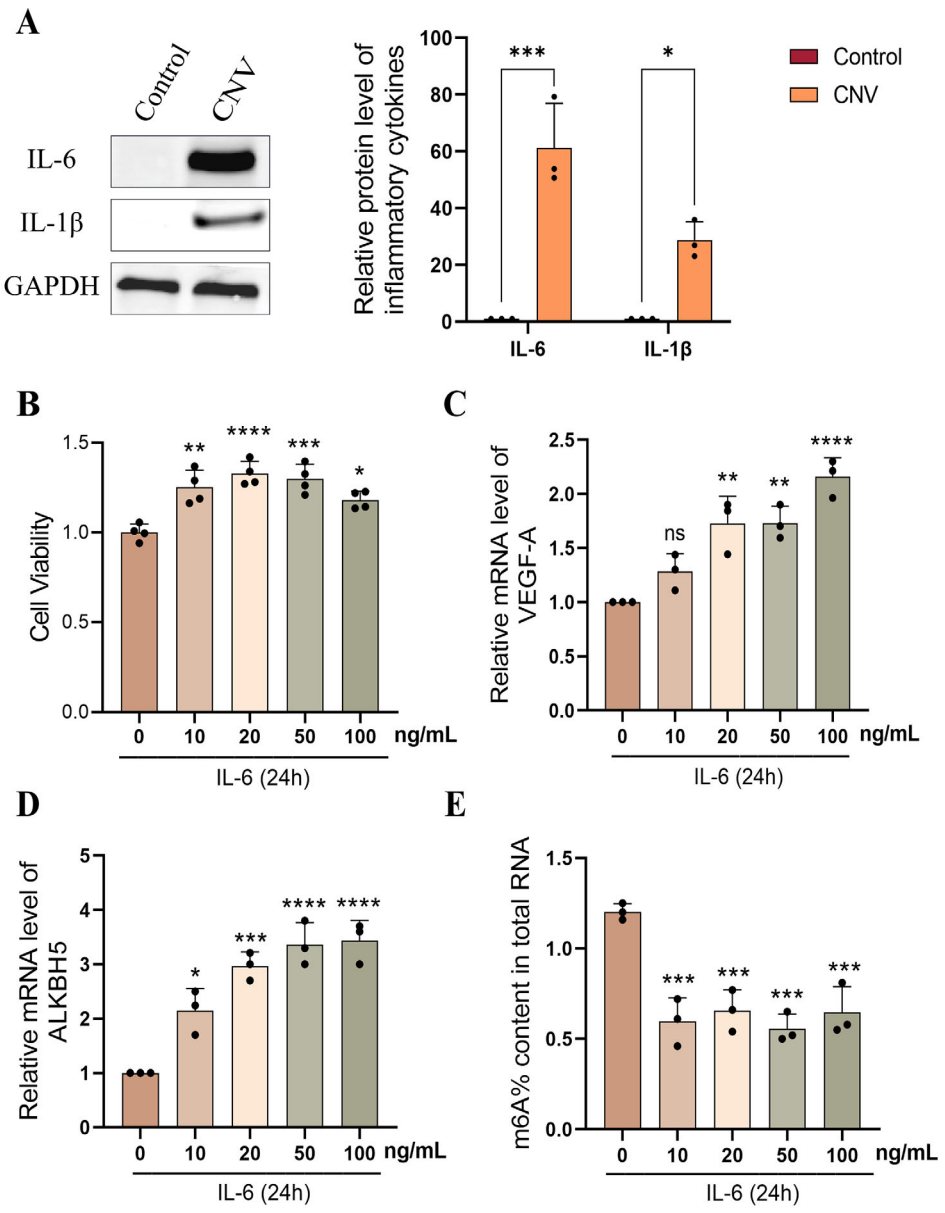

Figure 4. Downregulated m6A levels and upregulated ALKBH5 expression in IL-6-induced HUVECs. (**A**) Western blot analysis (*left graph*) and quantitative analysis (*right graph*) of IL-6 and IL-1β protein levels in normal and CNV corneas, with the fold ratio of the control group normalized to 1 ($n = 6$). (**B**) The CCK8 assay was used to analyze the cell viability of HUVECs treated with varying concentrations of IL-6 for 24 hours. (**C**) The qRT–PCR analysis of VEGF-A in HUVECs treated with different IL-6 concentrations for 24 hours, with the fold ratio of the control group normalized to 1. (**D**) The qRT–PCR analysis of ALKBH5 in HUVECs treated with different IL-6 concentrations for 24 hours, with the fold ratio of the control group normalized to 1. (**E**) Quantitative analysis of total m6A levels in HUVECs after 24-hour treatment with varying IL-6 concentrations. n is the total number of test animals used. *$P < 0.05$, **$P < 0.01$, ***$P < 0.001$, ****$P < 0.0001$; ns, no significant difference, compared with the control group.

Furthermore, siALKBH5 injection had no discernible impact on corneal epithelial thickness (Figs. 3C, 3F).

The expression levels of two proteins related to angiogenesis in each group were subsequently analyzed. Consistent with previous reports,[26] the western blot analyses showed a notable upregulation of VEGF-A and CD31 in neovascular corneas after alkali burns. Further knockdown of ALKBH5 effectively suppressed their expression (Fig. 3G). Similar trends were also observed in the IHF staining results (Figs. 3H, 3I). In summary, ALKBH5 inhibition can alleviate alkali burn-induced CNV, and its mediated m6A demethylation may play a role in the formation and progression of CNV.

Downregulated m6A Levels and Upregulated ALKBH5 Expression in IL-6–Induced HUVECs

Inflammation has been identified as a significant driving factor for the CNV progression. We examined the protein expression levels of inflammatory cytokines (IL-6 and IL-1β) in normal and neovascular corneas. The results showed that

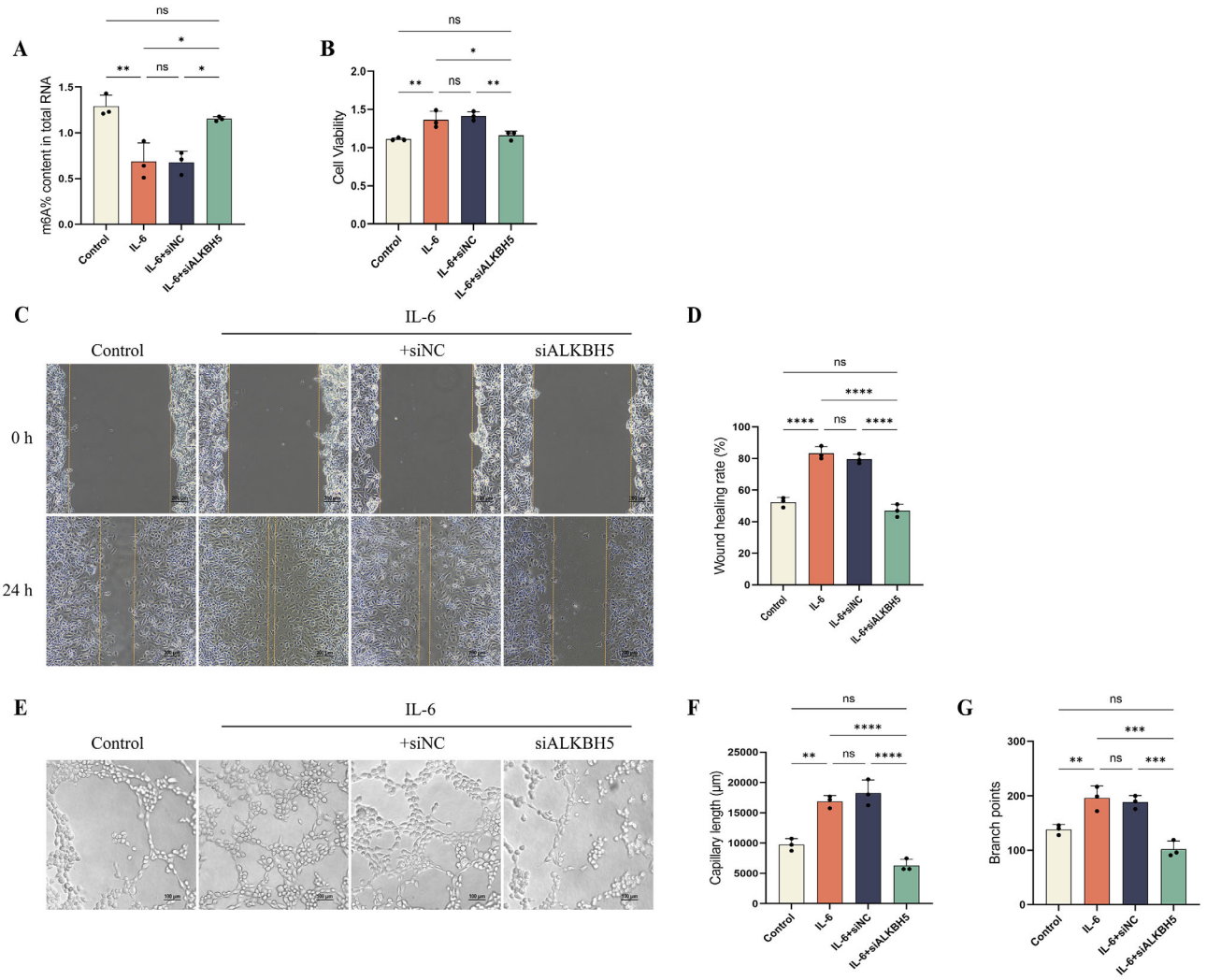

Figure 5. The anti-angiogenic effect of siALKBH5 in IL-6-induced HUVECs. (**A**) Quantitative analysis of total m6A levels in the control group, IL-6 group, IL-6 + siNC group, and IL-6 + siALKBH5 group. (**B**) The CCK8 assay was used to analyze the cell viability of HUVECs in four groups. (**C, D**) The images taken at 0 and 24 hours after scratching in the wound healing assay and the assessment of wound healing rates. *Scale bar:* 200 µm. (**E**) The formation of tubes was visualized after cell seeding on Matrigel and incubated for four hours in four groups. *Scale bar:* 100 µm. Quantification results of capillary lengths (**F**) and branch points (**G**). (**H**) Western blot analysis (*leftmost image*) and quantitative analysis (*right two images*) of VEGF-A and CD31 protein levels in four groups, with the fold ratio of the control group normalized to 1. (**I, J**) ICF analysis (*left graph*) and quantitative analysis (*right graph*) of VEGF-A and CD31 in four groups. The relative fluorescence intensity was determined by comparing the average fluorescence intensity values of the samples, expressed as folds relative to the control. VEGF-A and CD31, *red*; nucleus, *blue*. *Scale bar:* 50 µm. $^{*}P < 0.05$, $^{**}P < 0.01$, $^{***}P < 0.001$, $^{****}P < 0.0001$; ns, no significant difference.

in the CNV group, both IL-6 and IL-1β were significantly expressed, with a more prominent increase observed for IL-6 (Fig. 4A).

Therefore we stimulated HUVECs with different IL-6 concentrations for 24 hours to establish an in vitro model of angiogenesis. Results showed that IL-6 at concentrations of 10, 20, 50, and 100 ng/mL promoted cell proliferation, with 20 ng/mL being the most significant (Fig. 4B). Figure 4C shows that VEGF-A expression in IL-6-induced HUVECs significantly increased within the range of 20 to 100 ng/mL. Moreover, under IL-6 treatment at 10, 20, 50, and 100 ng/mL, ALKBH5 mRNA levels were upregulated, accompanied by a significant decrease in m6A methylation levels (Figs. 4D, 4E). Based on these findings, the subsequent in vitro modeling involved treating HUVECs with 20 ng/mL IL-6 for 24 hours.

The Anti-Angiogenic Effect of siALKBH5 in IL-6-Induced HUVECs

To investigate the specific effects of ALKBH5 in vitro, siALKBH5 and siNC plasmids were transfected into IL-6-induced HUVECs. The m6A quantitative analysis confirmed the increase in m6A content caused by ALKBH5 silencing (Fig. 5A). Notably, IL-6 significantly enhanced the proliferative, migratory, and tube-forming capabilities of HUVECs in CCK8 (Fig. 5B), wound healing (Figs. 5C, 5D), and tube formation assays (Figs. 5E–G). Silencing ALKBH5 exerted an opposite effect: reducing cell proliferation, inhibiting migration, and resulting in less tube formation. In addition, western blot (Fig. 5H) and ICF results (Figs. 5I, 5J) revealed that IL-6 stimulation significantly upregulated the expression of VEGF-A and CD31. Conversely, treatment with siALKBH5

Investigative Ophthalmology & Visual Science

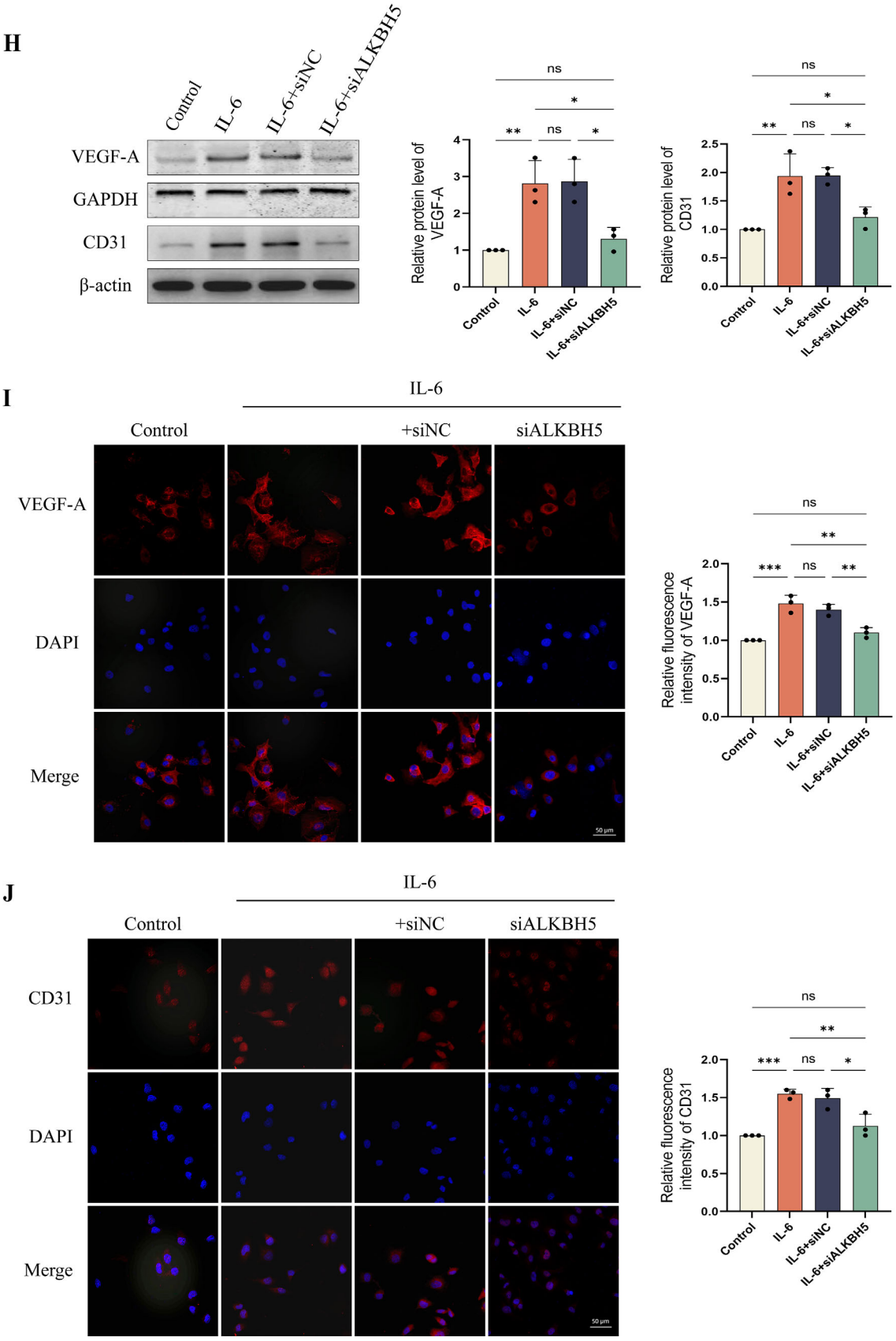

Figure 5. Continued.

Investigative Ophthalmology & Visual Science

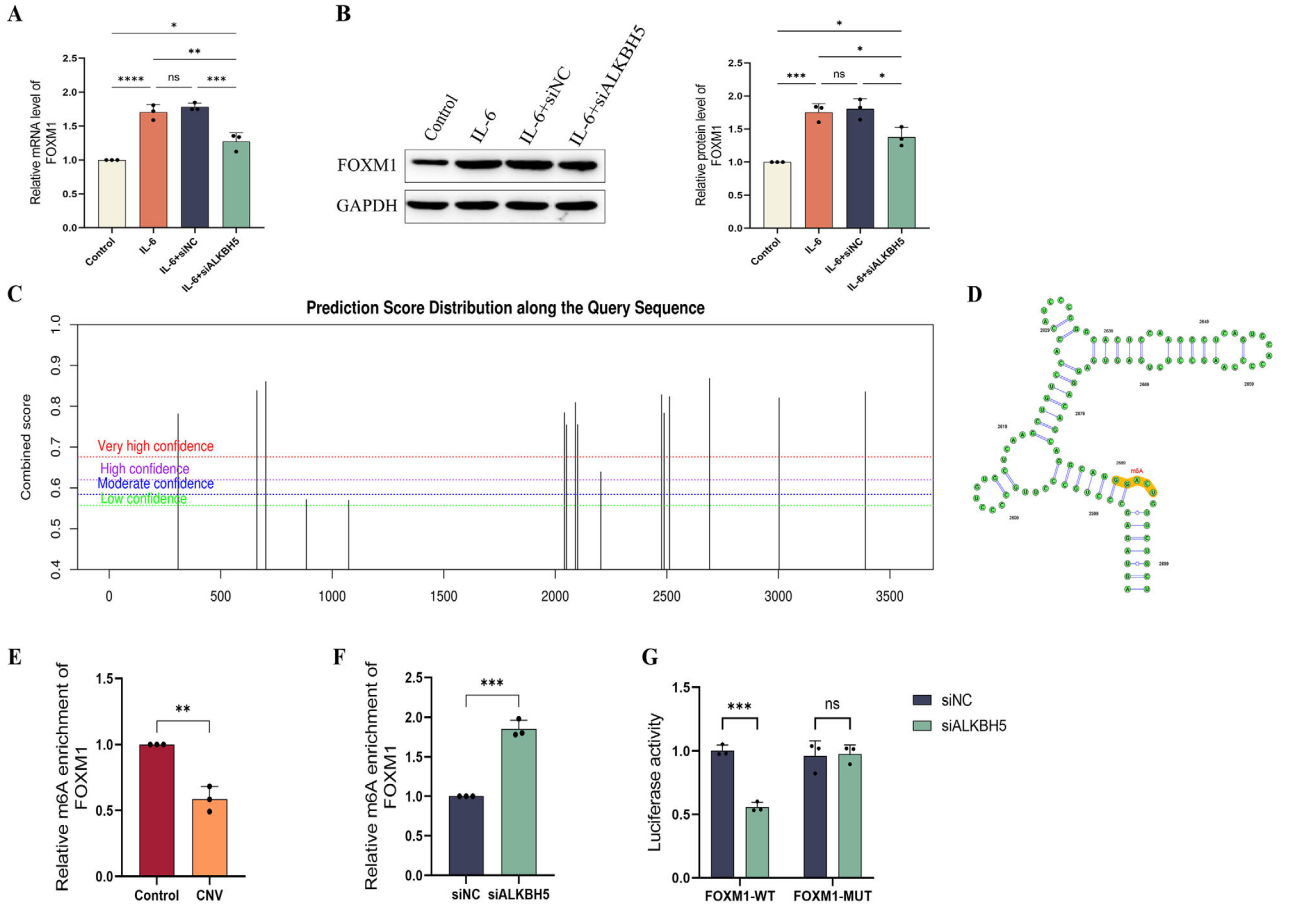

Figure 6. ALKBH5 mediates m6A modification of FOXM1. (**A**) The qRT–PCR analysis of FOXM1 in the control group, IL-6 group, IL-6 + siNC group, and IL-6 + siALKBH5 group, with the fold ratio of the control group normalized to 1. (**B**) Western blot analysis (*left graph*) and quantitative analysis (*right graph*) of FOXM1 protein levels in four groups, with the fold ratio of the control group normalized to 1. (**C**) The SRAMP online tool identified the m6A modification site on FOXM1 mRNA. The prediction results were sorted by position on the horizontal axis, and the vertical axis showed the combined prediction scores by three random forest classifiers. (**D**) The schematic of the most likely binding site generated by SRAMP. (**E**) MeRIP–qPCR analysis of FOXM1 m6A enrichment in normal and CNV corneas, with the fold ratio of the negative control normalized to 1. (**F**) MeRIP–qPCR analysis of FOXM1 m6A enrichment in IL-6-induced HUVECs with or without ALKBH5 knockdown, with the fold ratio of the negative control normalized to 1. (**G**) The interaction between ALKBH5 and FOXM1 using the dual-luciferase reporter assay in IL-6-induced HUVECs with or without ALKBH5 knockdown. *$P < 0.05$, **$P < 0.01$, ***$P < 0.001$, ****$P < 0.0001$; ns, no significant difference.

attenuated their expression levels. These findings emphasize the anti-angiogenic effect of siALKBH5, possibly mediated through m6A methylation modification in vitro.

ALKBH5 Mediates m6A Modification of FOXM1

It has been reported that m6A can be deposited on mRNAs that encode transcription factors, thereby influencing transcriptional regulation.[27] FOXM1, a transcriptional regulator of the cell cycle, can have its m6A mark on mRNA erased by ALKBH5 in some tumors.[21,28–30] The ALKBH5-FOXM1 axis control of CNV, however, had not been previously reported. Hence, FOXM1 expression was initially examined. The data revealed that FOXM1 was dramatically enhanced in IL-6–induced HUVECs, whereas ALKBH5 knockdown not only reduced FOXM1 mRNA levels but also protein levels (Figs. 6A, 6B).

Typically, each mRNA contains an average of one to three m6A modification sites.[31] The SRAMP analysis results revealed 16 m6A modification sites on FOXM1 mRNA, 13 of which have very high confidence, and the most likely binding site was at 2689–2693 on FOXM1 mRNA (Figs. 6C, 6D). From the above results, total m6A levels in the mouse CNV model were reduced. Here, using the MeRIP–qPCR analysis, we found that the decreased m6A levels on FOXM1 mRNA were easily detectable in CNV corneas compared to the control group (Fig. 6E). Moreover, MeRIP–qPCR analysis revealed that ALKBH5 knockdown increased the m6A levels of FOXM1 mRNA in IL-6-induced HUVECs (Fig. 6F). In addition, the dual-luciferase reporter assay showed that knocking down ALKBH5 significantly decreased the luciferase activity of the FOXM1-WT reporter gene but had no discernible effect on the FOXM1-MUT reporter gene, indicating the binding correlation between ALKBH5 and FOXM1 (Fig. 6G). These findings collectively suggest that ALKBH5 mediates m6A modification of FOXM1 in CNV.

FOXM1 Overexpression Reverses ALKBH5 Depletion Effects

To clarify the direct role of FOXM1 as an effector in CNV development mediated by ALKBH5, we conducted a rescue experiment by overexpressing FOXM1 in ALKBH5-

Investigative Ophthalmology & Visual Science

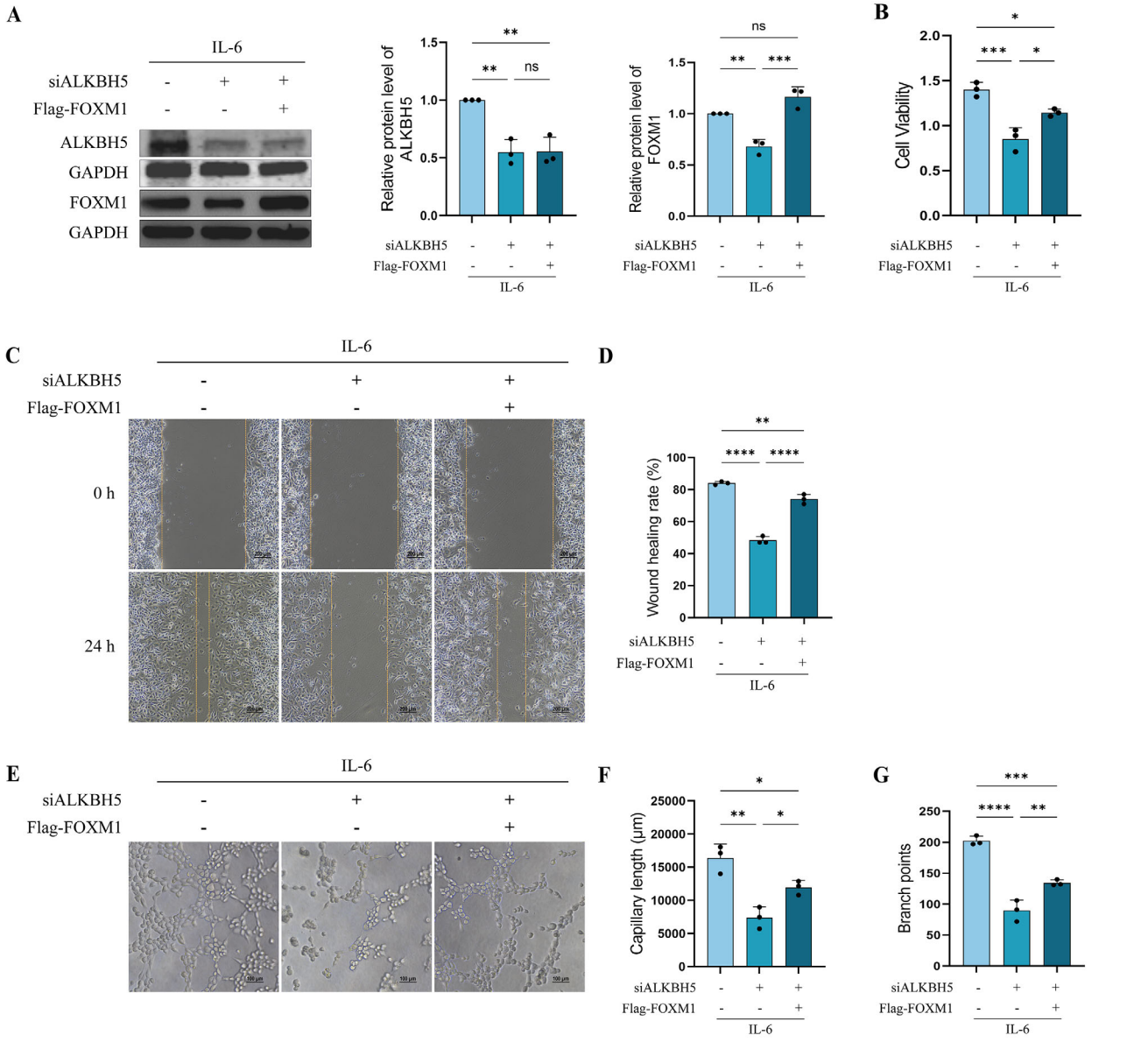

Figure 7. FOXM1 overexpression reverses ALKBH5 depletion effects. (**A**) Western blot analysis (*leftmost image*) and quantitative analysis (*right two images*) of ALKBH5 and FOXM1 protein levels, with the fold ratio of the control group normalized to 1. (**B**) The CCK8 assay was used to analyze the cell viability of HUVECs. (**C, D**) The images taken at 0 and 24 hours after scratching in the wound healing assay and the assessment of wound healing rates. *Scale bar:* 200 μm. (**E**) The formation of tubes was visualized after cell seeding on Matrigel and incubated for four hours. *Scale bar:* 100 μm. Quantification results of capillary lengths (**F**) and branch points (**G**). *$P < 0.05$, **$P < 0.01$, ***$P < 0.001$, ****$P < 0.0001$; ns, no significant difference.

depleted cells where FOXM1 levels were reduced (Fig. 7A). The results indicated that augmenting FOXM1 expression partially counteracted the impact of ALKBH5 depletion on the proliferation, migration, and tube formation of IL-6-induced HUVECs (Figs. 7B–G). Taken together, these data indicate that FOXM1 is a pivotal target for ALKBH5 in CNV.

Discussion

CNV is a substantial cause of vision loss and continues to be a major global public health concern. The lack of effective treatment strategies makes CNV challenging to cure, whereas its underlying pathogenesis remains unclear.[32] Presently, several animal models have been developed to study CNV, including corneal pocket assays, suture injury models, alkali burn models, and various transgenic models.[33] Consistent with our previous study, significant CNV was observed on the seventh day in the alkali burn model.[34] Alkali-burned corneas exhibit significant characteristic changes such as inflammation and neovascularization accompanied by the accumulation of inflammatory and pro-angiogenic factors (IL-1β, IL-6, and VEGF-A).[35] Among these factors, VEGF-A from the VEGF family has been identified as a significant pathogenic contributor to ocular neovascularization. Its angiogenic activity primarily binds to VEGFR-2, triggering receptor dimerization, autophosphorylation, and subsequent signal transduction that directs the cellular function.[36] Similarly, in this study, there was a significant devel-

Investigative Ophthalmology & Visual Science

opment of inflammatory cell infiltration and neovascularization seven days after corneal alkali damage, along with elevated expression of VEGF-A and CD31, which was also observed in IL-6-induced HUVECs.

As the most common internal modification of RNA, m6A extensively regulates RNA function in biological processes and diseases.[37] ALKBH5-mediated m6A modification can promote pathological angiogenesis in various diseases, including multiple myeloma,[14] choroidal neovascularization,[16] lung cancer,[38] and gastric cancer,[39] by promoting the secretion of VEGF-A, which is positively correlated with ALKBH5.[40] However, the regulatory mechanisms of ALKBH5 in CNV remain largely unknown. Our findings demonstrated that ALKBH5 expression correlated with changes in neovascularization area and length at three, seven, and 14 days after alkali burn and reached its peak at seven days. At this time point, m6A levels significantly decreased, with ALKBH5 emerging as the most prominently upregulated m6A-related enzyme, primarily expressed in corneal vascular endothelial cells. These observations suggest that ALKBH5-mediated demethylation modification is a crucial factor leading to abnormal m6A levels in CNV. Additionally, subconjunctival injection of siALKBH5 could alleviate CNV development and downregulate the expression of VEGF-A and CD31, indicating the angiogenesis-promoting effect of ALKBH5.

IL-6 is a potent stimulus for vessel sprouting and neovascularization.[41] Previous studies have demonstrated that during the early stages of corneal alkali burn injury, IL-6 is strongly induced and reaches its peak secretion on the seventh day,[42] a significant increase also observed at this time point in our findings. Therefore, HUVECs were stimulated with IL-6 to mimic CNV in vitro. As anticipated, the results showed that IL-6 promoted cell proliferation, migration, and tube formation, along with significantly increasing VEGF-A and CD31 expression in HUVECs. Additionally, we noted a decrease in overall m6A levels and an increase in ALKBH5 expression. These pro-angiogenic effects induced by IL-6 were attenuated when ALKBH5 was inhibited. Consistent with existing literature, ALKBH5 has been shown to be highly expressed in various tumors, and its depletion also inhibits the proliferation and migration ability of tumor cells.[38,40] In summary, ALKBH5-dependent m6A demethylation modification plays a crucial role in promoting CNV and may act as a potential indicator of CNV progression.

FOXM1 is a transcription factor belonging to the forkhead box family. It has a DNA-binding domain with a winged helix and can control the transcription of VEGF-A.[43] Previous research has indicated that FOXM1 can promote tumor angiogenesis.[44,45] FOXM1 is commonly overexpressed and is regulated by ALKBH5 in certain cancers, such as glioblastoma,[21] uveal melanoma,[28] lung adenocarcinoma,[29] and oral squamous cell carcinoma,[30] contributing to its tumorigenic properties. Here, we note that several positions have been predicted as m6A sites with very high confidence. Given the expected roles of m6A modification in controlling RNA structures and stability,[46] removing these m6A sites may damage the local structure and affect the stability of FOXM1 mRNA, which would be further investigated in the future. The data indicate that the expression levels of FOXM1 were upregulated in IL-6–induced HUVECs and correlated with proliferation, migration, and tube formation, as regulated by ALKBH5 demethylation. Moreover, ALKBH5 knockdown can elevate m6A levels in FOXM1 mRNA and suppress its transcription.

In conclusion, this work is the first, to the best of our knowledge, to elucidate the role of ALKBH5-mediated m6A demethylation in the process of CNV. Our findings revealed a noticeable decrease in m6A levels and elevated expression of ALKBH5 in both alkali burn-induced CNV and IL-6-induced HUVECs. Furthermore, the anti-angiogenic impact of inhibiting ALKBH5 is shown both in vivo and in vitro. Mechanically, ALKBH5 regulates CNV progression by modulating the m6A demethylation modification of FOXM1. However, some limitations should be acknowledged. First, we used siRNA to target ALKBH5 specifically. Before clinical applications, more validation using ALKBH5 gene knockout or overexpression animal models with CNV is warranted to strengthen these results. Second, m6A modification usually requires different m6A-binding proteins, including but not limited to the YT521-B homology (YTH) domain family and heterogeneous nuclear ribonucleoproteins, to further regulate the fate and function of target mRNAs.[47] Therefore the specific regions of FOXM1 mRNA undergoing m6A demethylation modification in CNV, as well as the types of m6A-binding proteins that bind to these modified regions, remain to be elucidated. Overall, our data strongly support a critical role for the ALKBH5-m6A-FOXM1 signaling axis in CNV and highlight ALKBH5 as a promising therapeutic target.

Acknowledgments

The authors thank Yefei Shi for assistance in revising the article, Huan Yu for experimental support, and Longxiang Yao for data support.

Supported by Project of Shanghai Science and Technology (20ZR1443600) and National Natural Science Foundation of China (82301162).

Disclosure: **W. Wang**, None; **H, Li**, None; **Y. Qian**, None; **M. Li**, None; **M. Deng**, None; **D. BI**, None; **J. Zou**, None

References

1. Feizi S, Azari AA, Safapour S. Therapeutic approaches for corneal neovascularization. *Eye Vision*. 2017;4:1–10.
2. Nicholas MP, Mysore N. Corneal neovascularization. *Exp Eye Res*. 2021;202:108363.
3. Yang YL, Zhong JM, Cui DM, Jensen LD. Up-to-date molecular medicine strategies for management of ocular surface neovascularization. *Adv Drug Deliv Rev*. 2023;201:115084.
4. Gupta D, Illingworth C. Treatments for corneal neovascularization: a review. *Cornea*. 2011;30:927–938.
5. Al-Debasi T, Al-Bekairy A, Al-Katheri A, Al Harbi S, Mansour M. Topical versus subconjunctival anti-vascular endothelial growth factor therapy (Bevacizumab, Ranibizumab and Aflibercept) for treatment of corneal neovascularization. *Saudi J Ophthalmol*. 2017;31:99–105.
6. Tan FH, Zhao MY, Xiong F, et al. N6-methyladenosine-dependent signalling in cancer progression and insights into cancer therapies. *J Exp Clin Canc Res*. 2021;40:146.
7. Huo F-C, Zhu Z-M, Du W-Q, et al. HPV E7-drived ALKBH5 promotes cervical cancer progression by modulating m6A modification of PAK5. *Pharmacol Res*. 2023;195.
8. Roignant JY, Soller M. m(6)A in mRNA: an ancient mechanism for fine-tuning gene expression. *Trends Genet*. 2017;33:380–390.
9. Bai Y, Jiao X, Hu J, Xue W, Zhou Z, Wang W. WTAP promotes macrophage recruitment and increases VEGF secretion via N6-methyladenosine modification in corneal

neovascularization. *Biochim Biophys Acta Mol Basis Dis.* 2023;1869:166708.
10. Shan K, R-m Zhou, Xiang J, et al. FTO regulates ocular angiogenesis via m(6)A-YTHDF2-dependent mechanism. *Exp Eye Res.* 2020;197:108107.
11. Wang W, Ye W, Chen S, et al. METTL3-mediated m6A RNA modification promotes corneal neovascularization by upregulating the canonical Wnt pathway during HSV-1 infection. *Cell Signal.* 2023;109:110784.
12. Yao M-D, Jiang Q, Ma Y, et al. Role of METTL3-dependent N-6-methyladenosine mRNA modification in the promotion of angiogenesis. *Mol Ther.* 2020;28:2191–2202.
13. Wang JY, Wang JQ, Gu Q, et al. The biological function of m6A demethylase ALKBH5 and its role in human disease. *Cancer Cell Int.* 2020;20:1–7.
14. Yu TT, Yao L, Yin H, Teng Y, Hong M, Wu QL. ALKBH5 promotes multiple myeloma tumorigenicity through inducing m(6)A-demethylation of SAV1 mRNA and myeloma stem cell phenotype. *Int J Biol Sci.* 2022;18:2235–2248.
15. Kumari R, Dutta R, Ranjan P, et al. ALKBH5 regulates SPHK1-dependent endothelial cell angiogenesis following ischemic stress. *Front Cardiovasc Med.* 2022;8:817304.
16. Sun R-X, Zhu H-J, Zhang Y-R, et al. ALKBH5 causes retinal pigment epithelium anomalies and choroidal neovascularization in age-related macular degeneration via the AKT/mTOR pathway. *Cell Rep.* 2023;42:112779–112779.
17. Halasi M, Gartel AL. Targeting FOXM1 in cancer. *Biochem Pharmacol.* 2013;85:644–652.
18. Wang R-T, Miao R-C, Zhang X, et al. Fork head box M1 regulates vascular endothelial growth factor-A expression to promote the angiogenesis and tumor cell growth of gallbladder cancer. *World J Gastroenterol.* 2021;27:692–707.
19. Zhang ZX, Xue ST, Gao Y, et al. Small molecule targeting FOXM1 DNA binding domain exhibits anti-tumor activity in ovarian cancer. *Cell Death Discov.* 2022;8(1):280.
20. Lan CL, Liu G, Huang LX, et al. Forkhead domain inhibitor-6 suppresses corneal neovascularization and subsequent fibrosis after alkali burn in rats. *Invest Ophthalmol Vis Sci.* 2022;63(4):14–14.
21. Zhang SC, Zhao BS, Zhou AD, et al. m(6)A Demethylase ALKBH5 maintains tumorigenicity of glioblastoma stem-like cells by sustaining FOXM1 expression and cell proliferation program. *Cancer Cell.* 2017;31:591–606.
22. Gottschalk B, Klec C, Leitinger G, et al. MICU1 controls cristae junction and spatially anchors mitochondrial Ca^{2+} uniporter complex. *Nat Commun.* 2019;10(1):3732.
23. Adler J, Parmryd I. Quantifying colocalization by correlation: the Pearson correlation coefficient is superior to the Mander's overlap coefficient. *Cytometry A.* 2010;77A:733–742.
24. Jabbari N, Nawaz M, Rezaie J. Bystander effects of ionizing radiation: conditioned media from X-ray irradiated MCF-7 cells increases the angiogenic ability of endothelial cells. *Cell Commun Signal.* 2019;17:1–12.
25. Zhou Y, Zeng P, Li YH, Zhang ZD, Cui QH. SRAMP: prediction of mammalian N6-methyladenosine (m6A) sites based on sequence-derived features. *Nucleic Acids Res.* 2016;44(10):e91–e91.
26. Shen T, Wu Y, Cai W, et al. LncRNA Meg3 knockdown reduces corneal neovascularization and VEGF-induced vascular endothelial angiogenesis via SDF-1/CXCR4 and Smad2/3 pathway. *Exp Eye Res.* 2022;222:109166.
27. Wei JB, He CA. Chromatin and transcriptional regulation by reversible RNA methylation. *Curr Opin Cell Biol.* 2021;70:109–115.
28. Hao L, Yin J, Yang H, et al. ALKBH5-mediated m(6)A demethylation of FOXM1 mRNA promotes progression of uveal melanoma. *Aging-Us.* 2021;13:4045–4062.
29. Chao Y, Shang J, Ji W. ALKBH5-m(6)A-FOXM1 signaling axis promotes proliferation and invasion of lung adenocarcinoma cells under intermittent hypoxia. *Biochem Biophys Res Commun.* 2020;521:499–506.
30. Shriwas O, Priyadarshini M, Samal SK, et al. DDX3 modulates cisplatin resistance in OSCC through ALKBH5-mediated m(6)A-demethylation of FOXM1 and NANOG. *Apoptosis.* 2020;25:233–246.
31. Boulias K, Greer EL. Biological roles of adenine methylation in RNA. *Nat Rev Genet.* 2023;24:143–160.
32. Zhang R, Yang J, Luo Q, Shi J, Xu H, Zhang J. Preparation and in vitro and in vivo evaluation of an isoliquiritigenin-loaded ophthalmic nanoemulsion for the treatment of corneal neovascularization. *Drug Deliv.* 2022;29:2217–2233.
33. Kather JN, Kroll J. Transgenic mouse models of corneal neovascularization: new perspectives for angiogenesis research. *Invest Ophthalmol Vis Sci.* 2014;55:7637–7651.
34. Wang W, Deng ML, Li M, Liu L, Zou J, Qian YY. Exploring corneal neovascularization: an integrated approach using transcriptomics and proteomics in an alkali burn mouse model. *Invest Ophthalmol Vis Sci.* 2024;65(1):21–21.
35. Li JD, Han JY, Shi YP, Liu MR. Rapamycin inhibits corneal inflammatory response and neovascularization in a mouse model of corneal alkali burn. *Exp Eye Res.* 2023;233:109539.
36. Cross MJ, Dixelius J, Matsumoto T, Claesson-Welsh L. VEGF-receptor signal transduction. *Trends Biochem Sci.* 2003;28:488–494.
37. Aufgebauer CJ, Bland KM, Horner SM. Modifying the antiviral innate immune response by selective writing, erasing, and reading of m6A on viral and cellular RNA. *Cell Chem Biol.* 2024;31:100–109.
38. Shen W, Pu J, Zuo Z, et al. The RNA demethylase ALKBH5 promotes the progression and angiogenesis of lung cancer by regulating the stability of the LncRNA PVT1. *Cancer Cell Int.* 2022;22(1):353.
39. Wang Q, Huang Y, Jiang M, et al. The demethylase ALKBH5 mediates ZKSCAN3 expression through the m 6 A modification to activate VEGFA transcription and thus participates in MNNG-induced gastric cancer progression. *J Hazard Mater.* 2024;473:134690.
40. Fan Y, Yan D, Ma L, et al. ALKBH5 is a prognostic factor and promotes the angiogenesis of glioblastoma. *Sci Rep.* 2024;14(1):1303.
41. Gopinathan G, Milagre C, Pearce OMT, et al. Interleukin-6 stimulates defective angiogenesis. *Cancer Res.* 2015;75:3098–3107.
42. Sotozono C, He JC, Matsumoto Y, Kita M, Imanishi J, Kinoshita S. Cytokine expression in the alkali-burned cornea. *Curr Eye Res.* 1997;16:670–676.
43. Monteiro LJ, Cubillos S, Sanchez M, et al. Reduced FOXM1 expression limits trophoblast migration and angiogenesis and is associated with preeclampsia. *Reprod Sci.* 2019;26:580–590.
44. Kim H, Park KJ, Ryu BK, et al. Forkhead box M1 (FOXM1) transcription factor is a key oncogenic driver of aggressive human meningioma progression. *Neuropathol Appl Neurobiol.* 2020;46:125–141.
45. Kuda M, Kohashi K, Yamada Y, et al. FOXM1 expression in rhabdomyosarcoma: a novel prognostic factor and therapeutic target. *Tumor Biol.* 2016;37:5213–5223.
46. Liu N, Dai Q, Zheng GQ, He C, Parisien M, Pan T. N6-methyladenosine-dependent RNA structural switches regulate RNA-protein interactions. *Nature.* 2015;518:560–564.
47. Zhao YC, Shi YF, Shen HF, Xie WZ. m6A-binding proteins: the emerging crucial performers in epigenetics. *J Hematol Oncol.* 2020;13:1–14.

Investigative Ophthalmology & Visual Science